Supplementary Information (SI) for Journal of Materials Chemistry B.

Supplementary Material

Biocompatible $NaLn(WO_4)_2$ core-shell nanoplatelets for multimodal MRI contrast, NIR imaging, and high sensitivity infrared luminescent ratiometric thermometry

Carlos Alarcón-Fernández,[a] Carlos Zaldo,[a] Manuel Bañobre-López,[b] Juan Gallo,[b] Pedro Ramos-Cabrer,[c,d] Sandra Plaza-García,[c] GonzaloVillaverde,[e] Alejandro Ruperti,[e] and Concepción Cascales[a*]

[a] Instituto de Ciencia de Materiales de Madrid, Consejo Superior de Investigaciones Científicas, c/ Sor Juana Inés de la Cruz 3, 28049 Madrid, Spain.
*Corresponding author, email: ccascales@icmm.csic.es
[b] Advanced (Magnetic) Theranostic Nanostructures Group INL—International Iberian Nanotechnology Laboratory, Av. Mestre José Veiga s/n, 4715-330 Braga, Portugal.
[c] CIC biomaGUNE, Basque Research and Technology Alliance, Paseo Miramón 194, 20014, Donostia-San Sebastián, Spain.
[d] Ikerbasque, Basque Foundation for Science, Plaza Euskadi 5, 48009 Bilbao, Spain.
[e] MatNaBio Group, Departamento de Química en Ciencias Farmacéuticas, Universidad Complutense de Madrid, Plaza Ramón y Cajal 2, 28040 Madrid, Spain.

CONTENT

Synthesis and purification of C@1S@2S and C@1S@2S@i3S.

Characterization of nanoprobes prepared by coprecipitation:

- **Figures S1a, S1b, S1c and S1d**: RT X-ray diffraction patterns of C, C@1S, C@1S@2S and C@1S@2S@i3S, respectively, including corresponding Scherrer d_S sizes.
- **Figures S2, S3, S4 and S5:** DLS plots of hydrodynamic sizes and size distributions of C, C@1S, C@1S@2S and C@1S@2S@i3S, respectively, dispersed in hexane and in water.
- **Table S1**: ICP-OES concentrations of Lns in water dispersions of C, C@1S, C@1S@2S and C@1S@2S@i3S.
- **Table S2**: ICP-OES concentrations of Lns in water dispersions of C@1S-b and C@1S-b@2S-b.
- **Table S3**: Comparison of ratios between concentrations of Gd and other Lns (Ho, Nd) in C@1S, C@1S-b, C@1S@2S and C@1S-b@2S-b.

Plots of relaxation rates R_1 and R_2 vs the concentration of the corresponding lanthanide:

- **Figure S6**: Plots of R_1 vs [Gd], and R_2 vs [Ho] for C, C@1S and C@1S@2S nanoprobes dispersed in water at 1.5 T magnetic field.
- **Figure S7**: Plots of R_1 vs [Gd] and R_2 vs [Ho] for C, C@1S and C@1S@2S nanoprobes dispersed in water at 7 T magnetic field.
- **Figure S8**: Plots of R_1 vs [Gd] and R_2 vs [Ho] for C, C@1S and C@1S@2S nanoprobes dispersed in water at 11.74 T magnetic field.
- **Figure S9**: Plots of R_1 vs [Gd] and R_2 vs [Ho] for C@1S-b and C@1S-b@2S-b nanoprobes dispersed in water at 3 T magnetic field.

Plots of measured magnetization of C, C@1S and C@1S@2S vs magnetic field H: Figure S10.

Nd and Yb-codoped $NaGd(WO_4)_2$ polycrystalline samples prepared by solid state synthesis (SSS): Synthesis procedure and characterization

- Description of solid state syntheses and composition of prepared samples.
- **Figure S11**: Room temperature X-ray patterns of samples prepared by solid state synthesis.

Figure S12. Thermal evolution of *LIR* Yb/Nd of SSS sample with composition 7.5 at%Nd:7.5 at%Yb:$NaGd(WO_4)_2$, λ_{EXC} = 803.4 nm.

Figures S13 and S14*:* Fluorescence microscopy images of HeLa and MC3T3 cells, respectively, stained with DAPI: comparison between control cells and cultured cells with water dispersions of different concentrations of the C@1S@2S@i3S nanoprobe.

Synthesis and purification of NaHo(WO_4)$_2$@8 at% Tm:15 at% Yb:NaGd(WO_4)$_2$@30 at% Nd: 20 at% Yb:NaGd(WO_4)$_2$ (C@1S@2S)

For the preparation of 0.4 mmol of C@1S@2S NPs, 1 mL of GdAc, 400 µL (600 µL, for the material with 30 at% Nd) of NdAc and 400 µL of YbAc from corresponding 0.2 M solutions were mixed with 12 mL ODE and 8 mL OA in a three-neck flask, and the solution was heated at 150 ºC (423 K) for 2 h under N_2 flow. After cooling down to 50 ºC (323 K), 0.3 mL of NaOH 2 M and 281 mg of $W(CO)_6$ were added, and this 2S-precursor solution was kept at this temperature for 2 h under strong stirring and N_2 flow. In other flask, about 0.1 mmol of previously prepared C@1S NPs (see main text) dispersed in n-hexane were mixed with 12 mL ODE, 8 mL OA and 8 mL OLE. The solutions of the two flasks were degasified by heating them to 100 ºC (373 K) under vacuum for 15 minutes or until they are both transparent. Then, after the controlled slow pouring of the 2S-precursor solution into the solution containing C@1S NPs, the synthesis procedure, the extraction and purification of C@1S@2S NPs were carried out under the same experimental conditions described in the main text for C@1S. The solution in n-hexane of achieved C@1S@2S NPs presents a bluish color.

For the preparation of C@1S-b@2S-b, the amount of the 2S-precursor was reduced to 3/4 of what was previously indicated.

Synthesis and purification of NaHo(WO_4)$_2$@8 at% Tm:15 at% Yb:NaGd(WO_4)$_2$@30 at% Nd: 20 at% Yb:NaGd(WO_4)$_2$@NaGd(WO_4)$_2$ (C@1S@2S@i3S)

To prepare 0.5 mmol of C@1S@2S@i3S NPs, the initial synthesis of the optically transparent NaGd(WO_4)$_2$ i3S-precursor solution required 2.5 mL of 0.2 M GdAc, that mixed with 12 mL ODE and 8 mL OA was heated at 150 ºC (423 K) during 2 h, under N_2 flow with gentle stirring. After cooling down at 50 ºC (323 K), 0.375 mL of 2M NaOH and 351 mg of $W(CO)_6$ were added to the above transparent oleate-capped Gd-containing solution, which was maintained at this temperature for 2 h under N_2 flow and strong stirring. In the second flask, we mixed about 0.35 mmol of previously prepared C@1S@2S [with 2S = 30 at% Nd:20 at% Yb:NaGd(WO_4)$_2$] NPs dispersed in n-hexane with 12 mL ODE, 8 mL OA and 8 mL OLE. After complete degassing of both solutions under vacuum at 100 ºC (373 K), and the slow addition of the i3S-precursor solution into the flask containing C@1S@2S NPs, the coprecipitation procedure for achieving C@1S@2s@i3S NPs, and their extraction and purification, were performed under the same experimental conditions already described. The solution in n-hexane of C@1S@2s@i3S NPs presents a slightly bluish color.

Characterization of nanoprobes prepared by coprecipitation

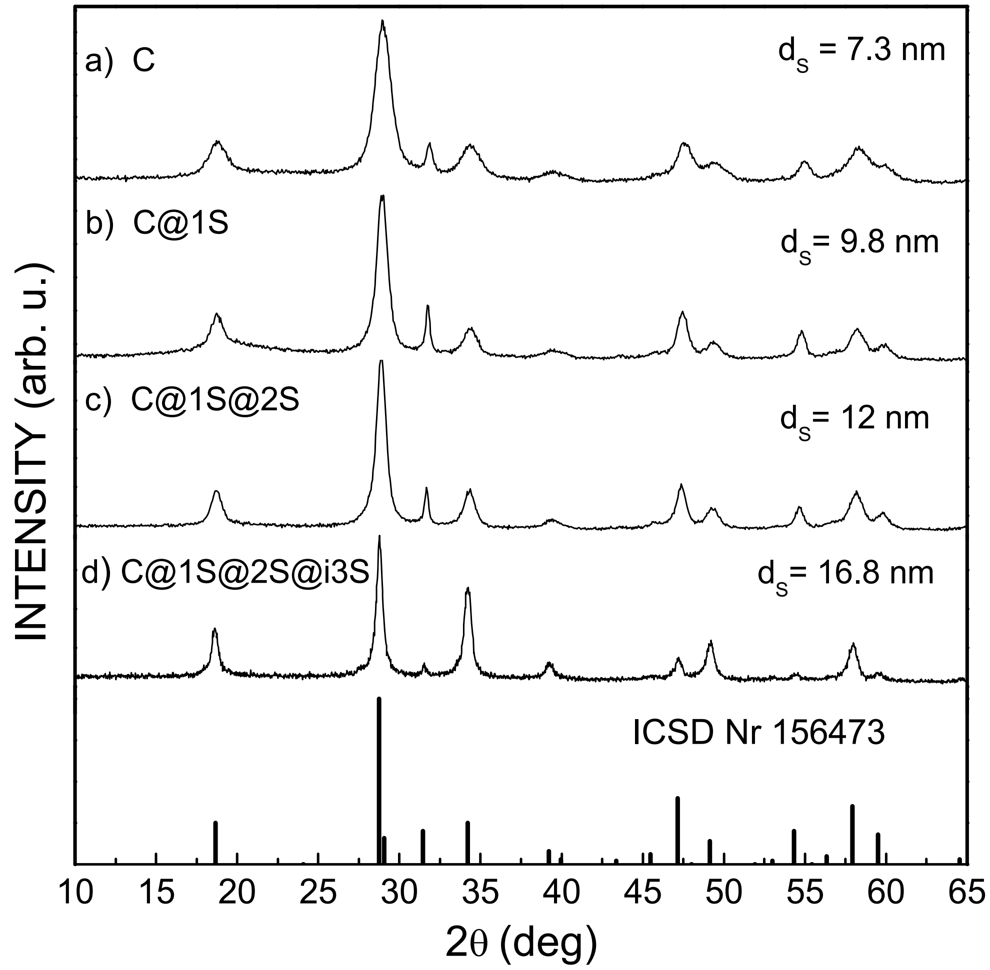

Figure S1. Room temperature X-ray diffraction patterns of a) C, b) C@1S, c) C@1S@2S and d) C@1S@2S@i3S nanoprobes synthesized by coprecipitation. Mean domain crystalline size calculated by the Scherrer' equation, d_S, is indicated for each material. For comparative purpose, the ICSD file #156473 corresponding to 17 at% Yb:NaGd$(WO_4)_2$ single crystal with the tetragonal scheelite-like phase is included (see also C. Cascales, M.D. Serrano, F. Esteban-Betegón, C. Zaldo, R. Peters, K. Petermann, G. Huber, L. Ackermann, D. Rytz, C. Dupré, M. Rico, J. Liu, U. Griebner, V. Petrov, *Phys. Rev. B* **2006**, *74*, 174114, reference 61 in the main text).

Sizes and size distribution by DLS of C, C@1S, C@1S@2S and C@1S@2S@i3S

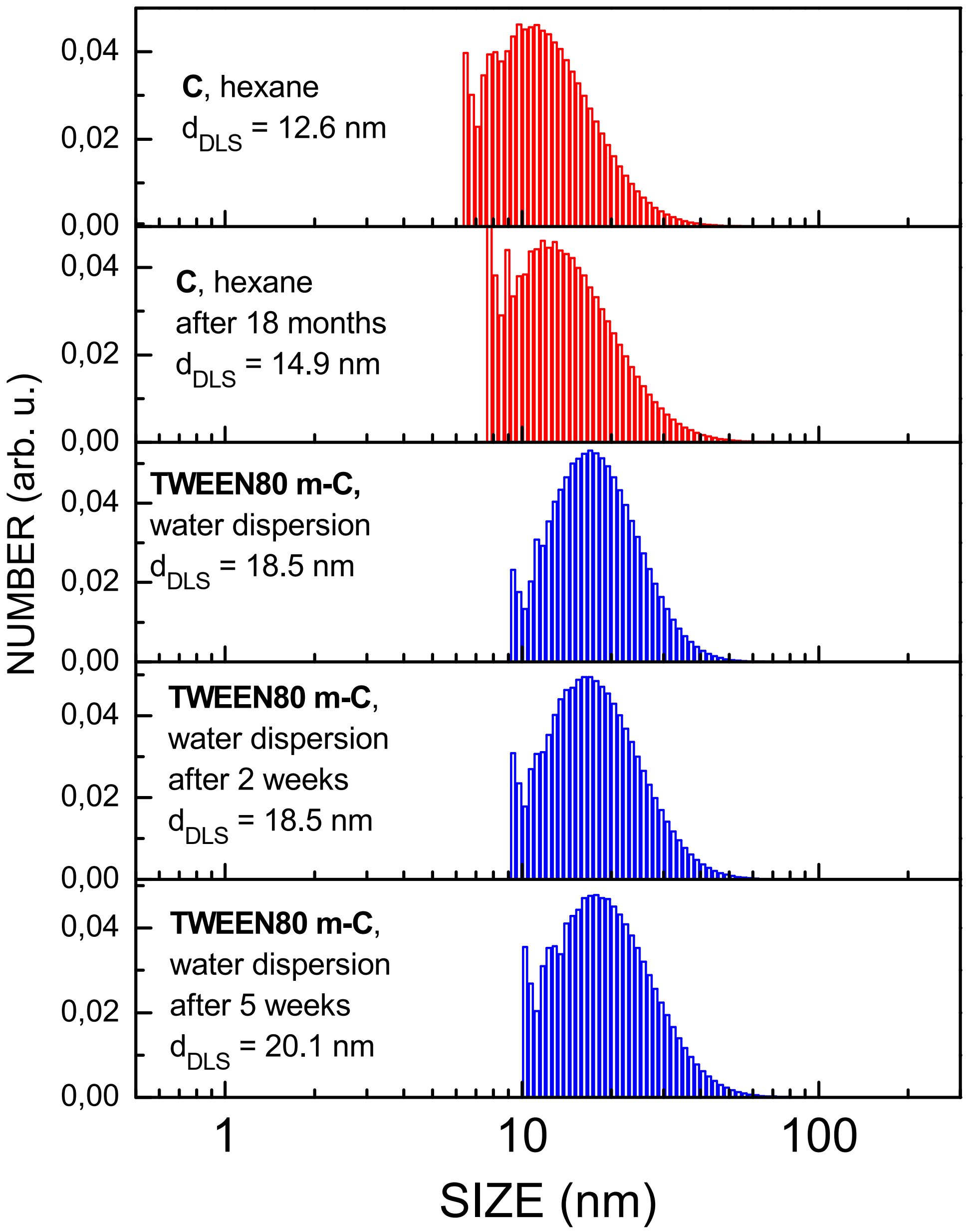

Figure S2. Dynamic Light Scattering plots of size distributions of $NaHo(WO_4)_2$, C, nanoparticles dispersed in hexane, and in water after surface modification with TWEEN80.

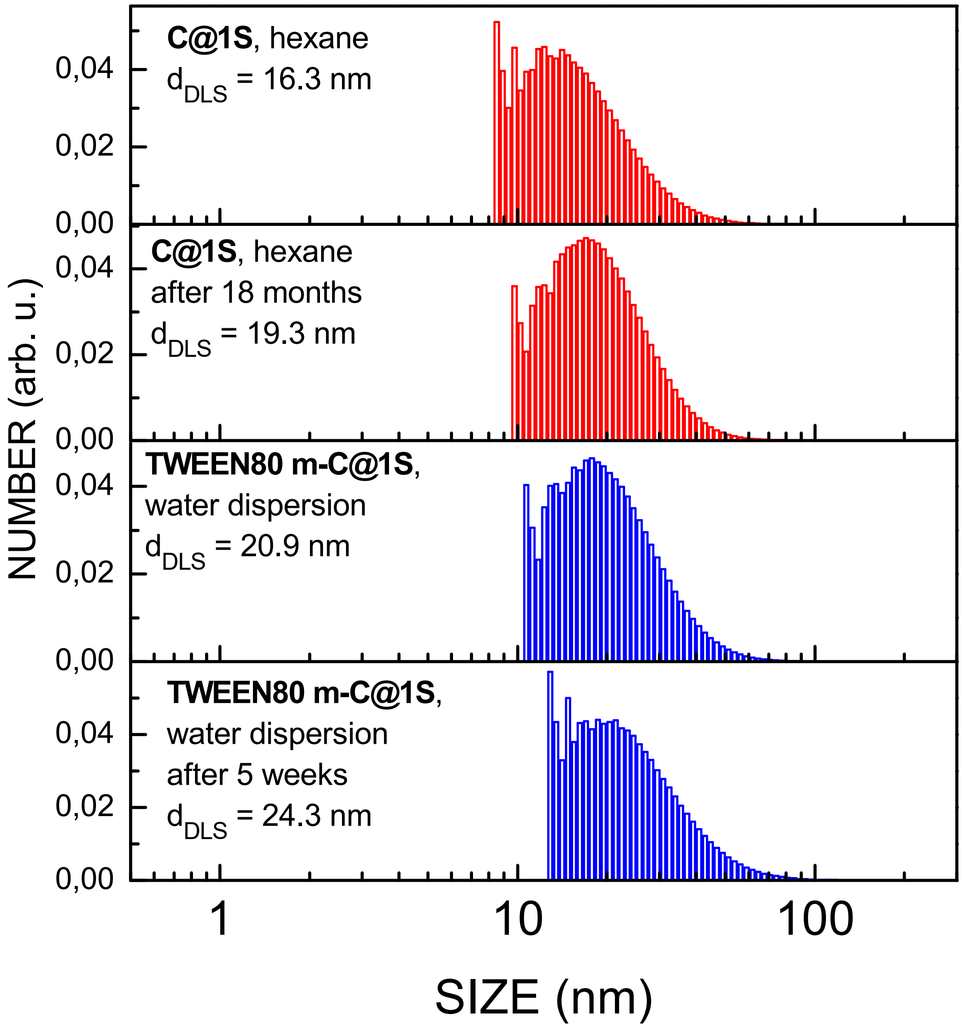

Figure S3. Dynamic Light Scattering plots of size distributions of NaHo$(WO_4)_2$@8 at%Tm,15at%Yb:NaGd$(WO_4)_2$, C@1S, dispersed in hexane, and in water after surface modification with TWEEN80.

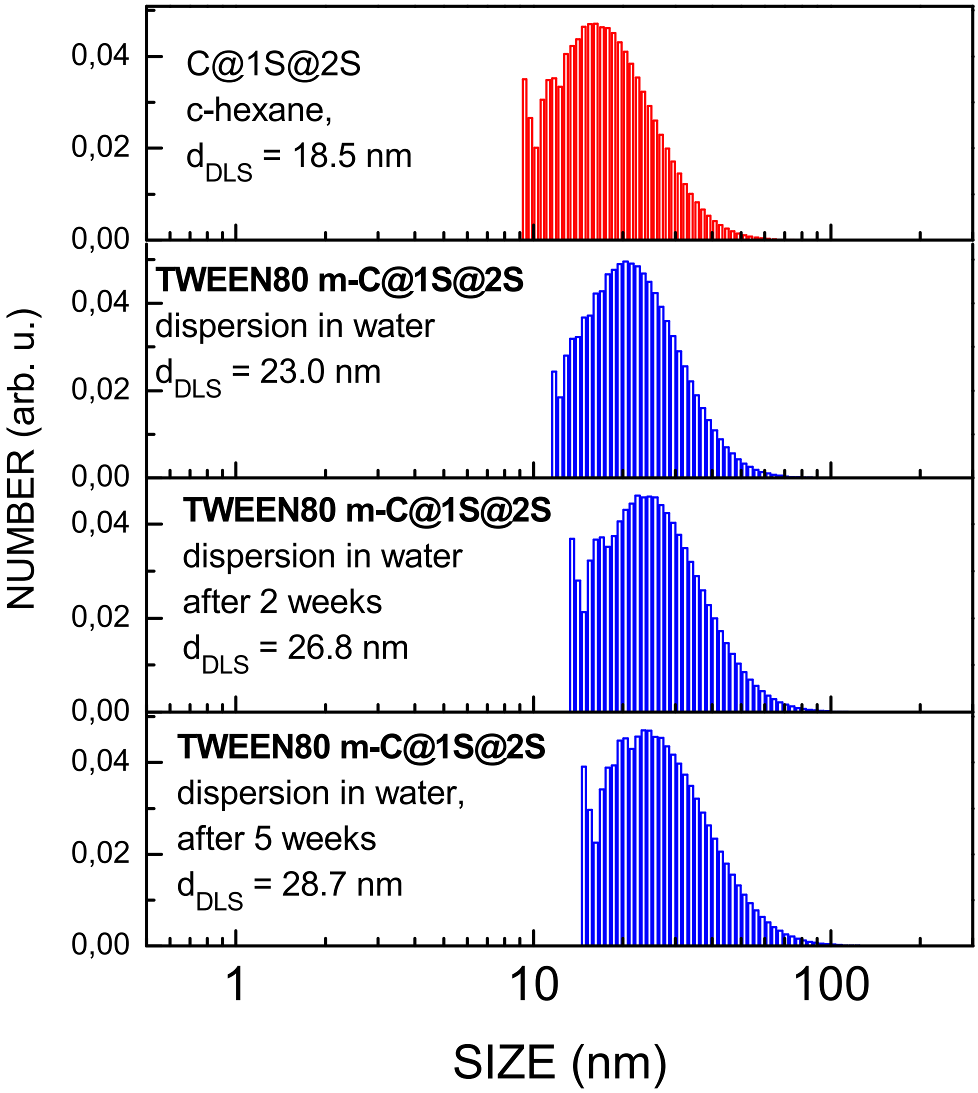

Figure S4. Dynamic Light Scattering plots of size distributions of NaHo$(WO_4)_2$@8 at%Tm,15at%Yb:NaGd$(WO_4)_2$@30at%Nd, 20at%Yb:NaGd$(WO_4)_2$, C@1S@2S, dispersed in hexane, and in water after surface modification with TWEEN80.

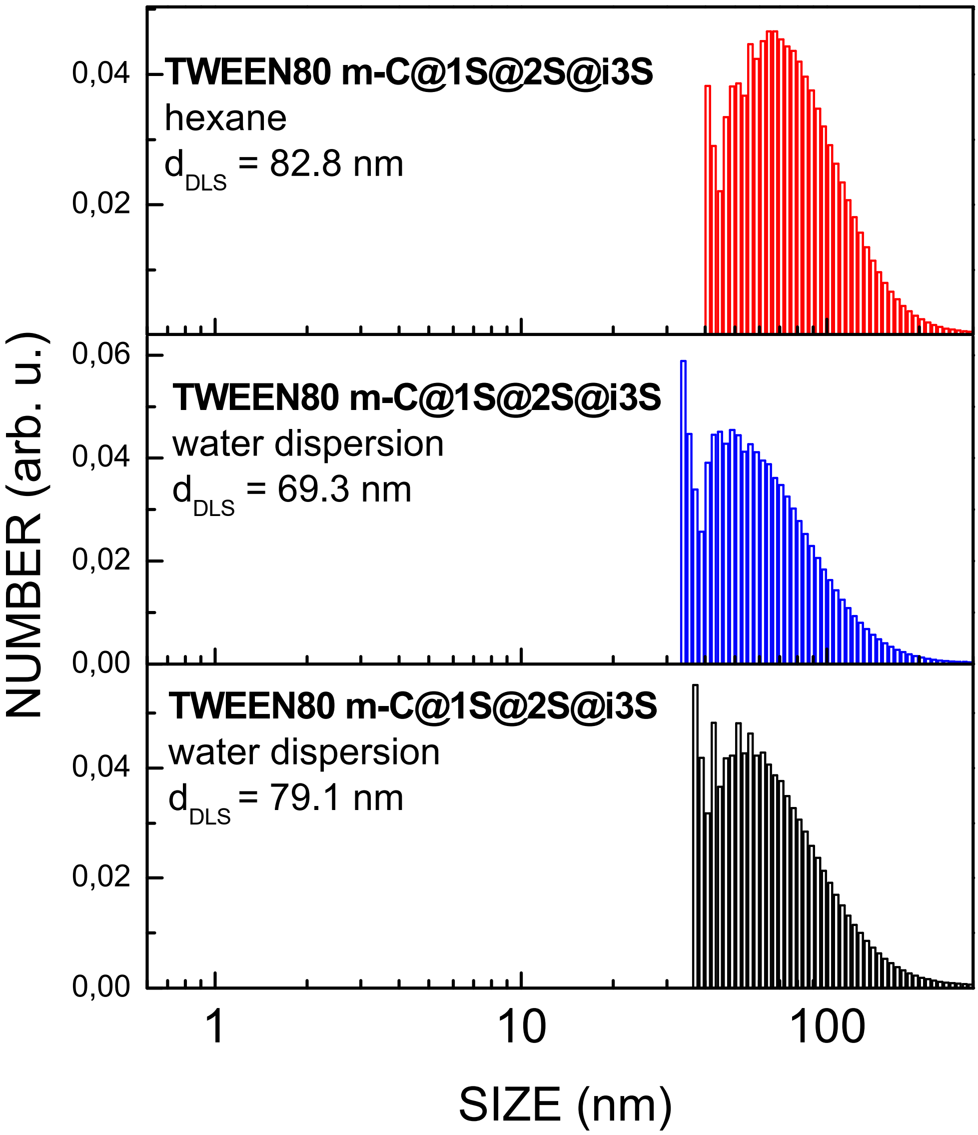

Figure S5. Dynamic Light Scattering plots of size distributions of NaHo$(WO_4)_2$@8 at% Tm,15at%Yb:NaGd$(WO_4)_2$@30at%Nd,20at%Yb:NaGd$(WO_4)_2$@NaGd$(WO_4)_2$, C@1S@2S@i3S, dispersed in hexane, and in water after surface modification with TWEEN80.

Table S1 ICP-OES concentrations of Lns in water dispersions of double tungstate-based nanoprobes. Units for given data are mmol/L, first row, and ×10^{17} at/cm^3, second row.

	Ho^{3+}	Gd^{3+}	Yb^{3+}	Tm^{3+}	Nd^{3+}
C	3.077/ 18.530	- -	- -	- -	- -
C@1S	0.255/ 1.536	0.216/ 1.300	0.011/ 0.066	0.007/ 0.042	- -
C@1S@2S	0.831/ 5.004	1.570/ 9.455	0.161/ 0.970	0.030/ 0.181	0.471/ 2.836
C@1S@2S@i3S	0.084/ 0.503	0.296/ 1.783	0.010/ 0.063	7.4×10^{-4}/ 4.5×10^{-3}	0.051/ 0.305

Table S2 ICP-OES concentrations of Lns in water dispersions of C@1S-b and C@1S@2S-b nanoprobes. Units for given data are mmol/L, first row, and ×10^{17} at/cm^3, second row.

	Ho^{3+}	Gd^{3+}	Yb^{3+}	Tm^{3+}	Nd^{3+}
C@1S-b	4.288/ 25.822	4.829/ 29.080	1.201/ 7.232	0.333/ 2.005	- -
C@1S-b@2S-b	6.594/ 39.709	16.429/ 98.935	2.835/ 17.072	0.588/ 3.541	3.674/ 22.125

Table S3 Relationships between concentrations of Gd and those of other Lns (Ho, Nd) in C@1S, C@1S-b, C@1S@2S and C@1S-b@2S-b nanoprobes.

	Gd:Ho	Gd:Nd	Gd:Ho+Nd
C@1S	1:1.18	-	
C@1S-b	1:0.88	-	
C@1S@2S	1:0.53	1:0.30	1:0.83
C@1S-b@2S-b	1:0.40	1:0.22	1:0.62

Plots of relaxation rates R_1 and R_2 versus the concentration of the corresponding lanthanide

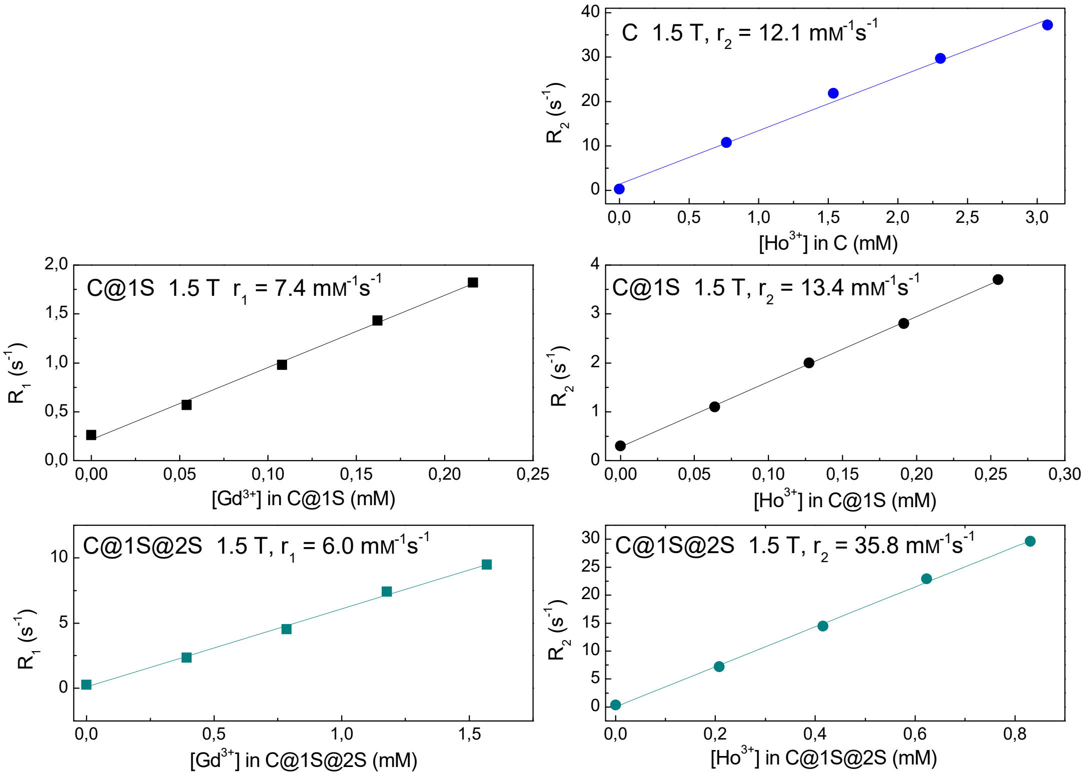

Figure S6. Calculations of r_1 and r_2 relaxivities (slope of the corresponding linear regression) for C, C@1S and C@1S@2S nanoprobes dispersed in water at 1.5 T magnetic field.

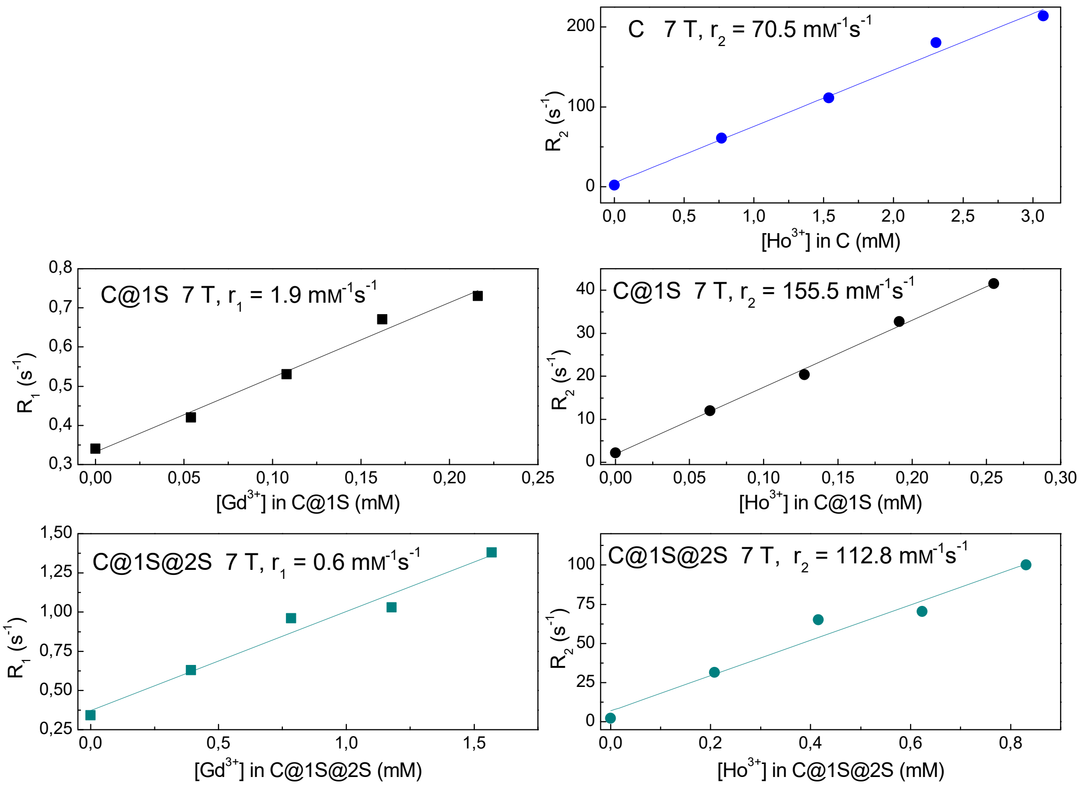

Figure S7. Calculations of r_1 and r_2 relaxivities (slope of the corresponding linear regression) for C, C@1S and C@1S@2S nanoprobes dispersed in water at 7 T magnetic field.

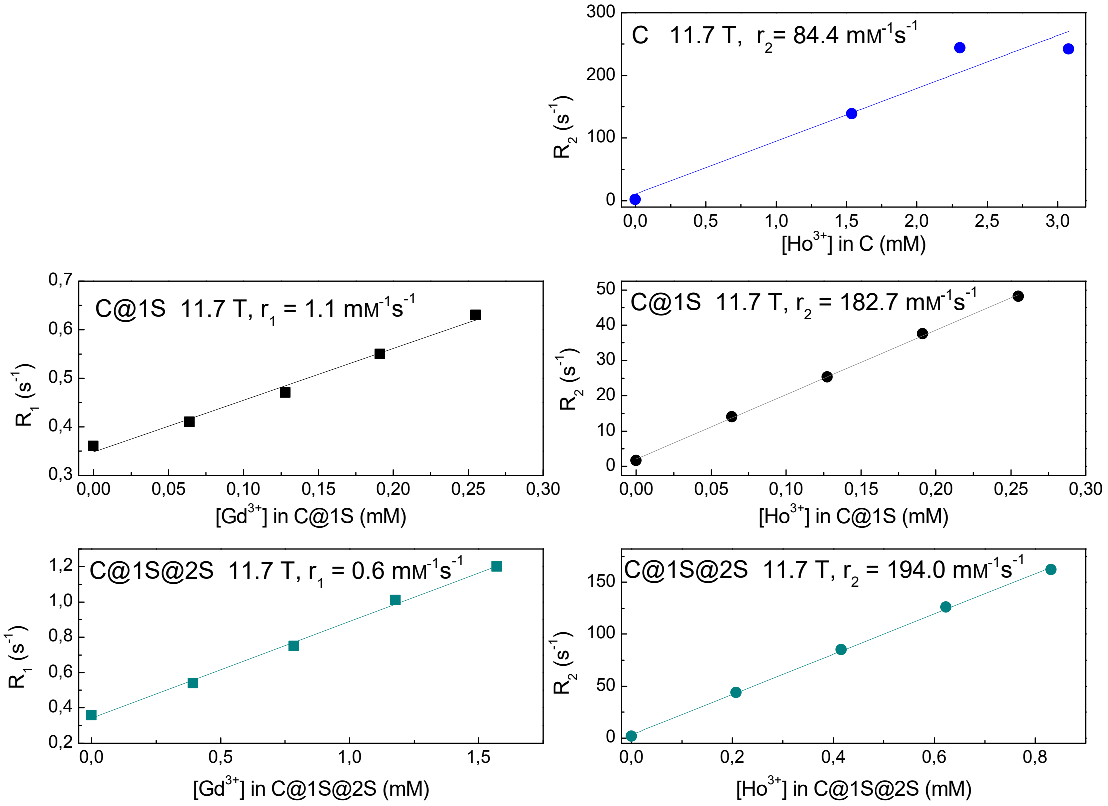

Figure S8. Calculation of r_1 and r_2 relaxivities (slope of the corresponding linear regression) for C, C@1S and C@1S@2S nanoprobes dispersed in water at 11.7 T magnetic field.

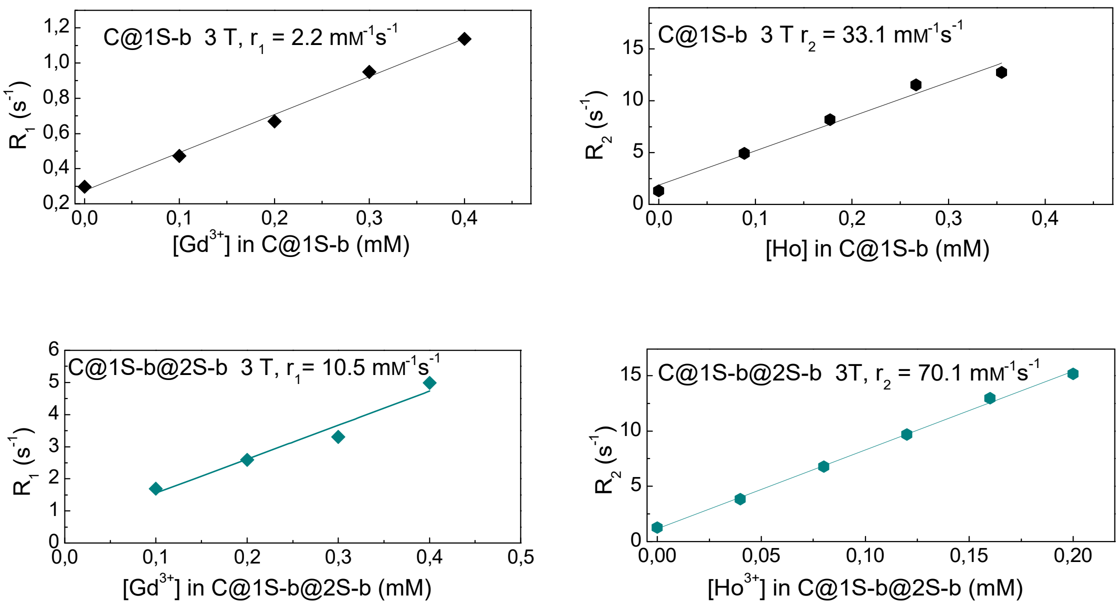

Figure S9. Calculation of r_1 and r_2 relaxivities (slope of the corresponding linear regression) for C@1S-b and C@1S-b@2S-b nanoprobes dispersed in water at 3 T magnetic field.

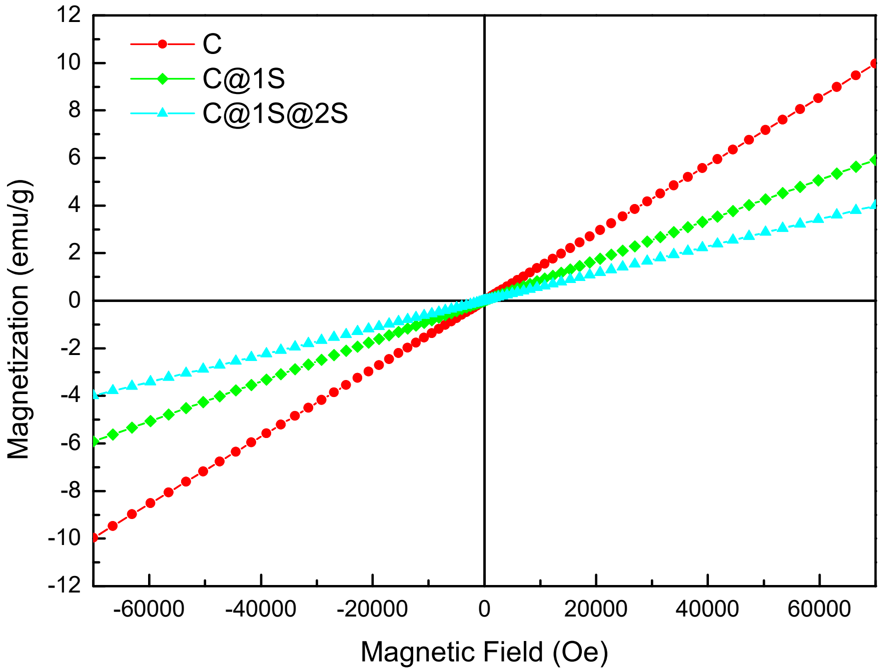

Figure S10. Plots of the magnetization values of C, C@1S and C@1S@2S vs the magnetic field H.

Nd and Yb-codoped $NaGd(WO_4)_2$ polycrystalline samples prepared by solid state synthesis (SSS): Synthesis procedure and characterization

Yb-doped and Nd and Yb-codoped $NaGd(WO_4)_2$ polycrystalline samples prepared by solid state synthesis (SSS)

Two series with compositions x at% Nd:y at% Yb:$NaGd(WO_4)_2$:
i) $x = 2, 10, 15, 17.5, 20, 22.5, 25, 30$; $y = 20$ in all cases.
ii) $x = y = 0.25, 0.5, 1, 2.5$, and 7.5
were prepared by SSS to obtain a previous knowledge of the best range of Yb^{3+} and Nd^{3+} doping levels in tetragonal scheelite-like double tungstates, to be used for contactless NIR-NIR temperature sensing studies.

Furthermore, single doped $NaGd_{1-x}Yb_x(WO_4)_2$ polycrystalline samples, $x = 0.01$, 0.05, 0.10, 0.20, were also prepared by SSS to be used as references in the evaluation of the Yb^{3+} PL intensity contribution at λ=1058 nm in each case, in order to discount this contribution in the evaluation of the Nd^{3+} PL intensity.

Na_2CO_3 (Alfa Aesar, 99.5%), WO_3 (Alfa Aesar, 99.8%), Yb_2O_3 (Strem Chemicals, 99.9%), Gd_2O_3 (Thermo Scientific Chemicals, 99.999%) and Nd_2O_3 (acquired through Shanghai Zimei International Co LTD, 99.99%) were used as reagents. The required stoichiometric mixtures for each sample were homogenized and firstly heated in air at 750 ºC (1023 K) for 15 h, cooled down to room temperature, ground, and then heated at 870 ºC (1143 K) for 24 h. X-ray diffraction analyses of final products indicated that they were in all cases pure-phase and highly crystalline tetragonal scheelite-like materials, isostructural with Yb:$NaGd(WO_4)_2$ crystals (C. Cascales, M. D. Serrano, F. Esteban-Betegón, C. Zaldo, R. Peters, K. Petermann, G. Huber, L. Ackermann, D. Rytz, C. Dupré, M. Rico, J. Liu, U. Griebner, V. Petrov, *Phys. Rev. B* **2006**, *74*, 174114; ICSD FIZ-Karlsruhe Nrs 156471-156474), see Figure S11.

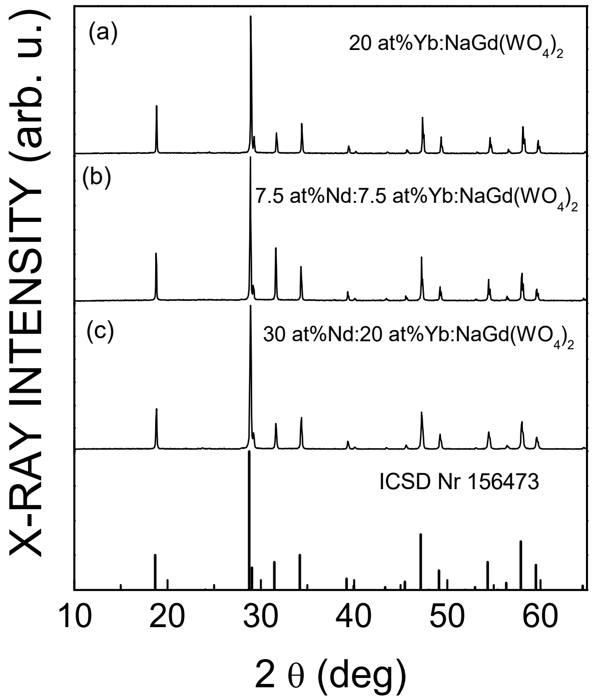

Figure S11. Room temperature X-ray diffraction patterns of selected compositions of Yb-doped (a) or (b) and (c) Nd and Yb-codoped NaGd(WO$_4$)$_2$ polycrystalline samples prepared by solid state synthesis.

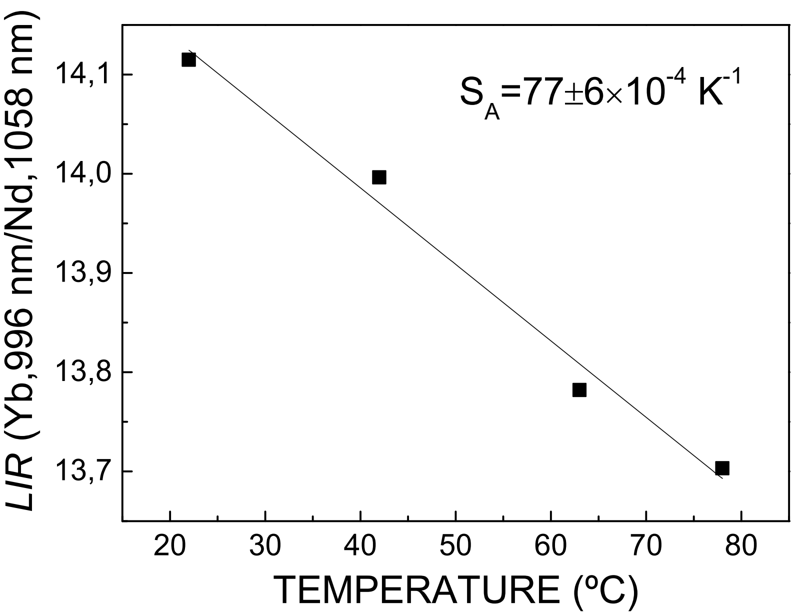

Figure S12. Thermal evolution of *LIR* Yb/Nd for the SSS sample with composition 7.5 at%Nd:7.5 at%Yb:NaGd(WO$_4$)$_2$, λ_{EXC}= 803.4 nm.

Fluorescence microscopy images of HeLa cells stained with DAPI

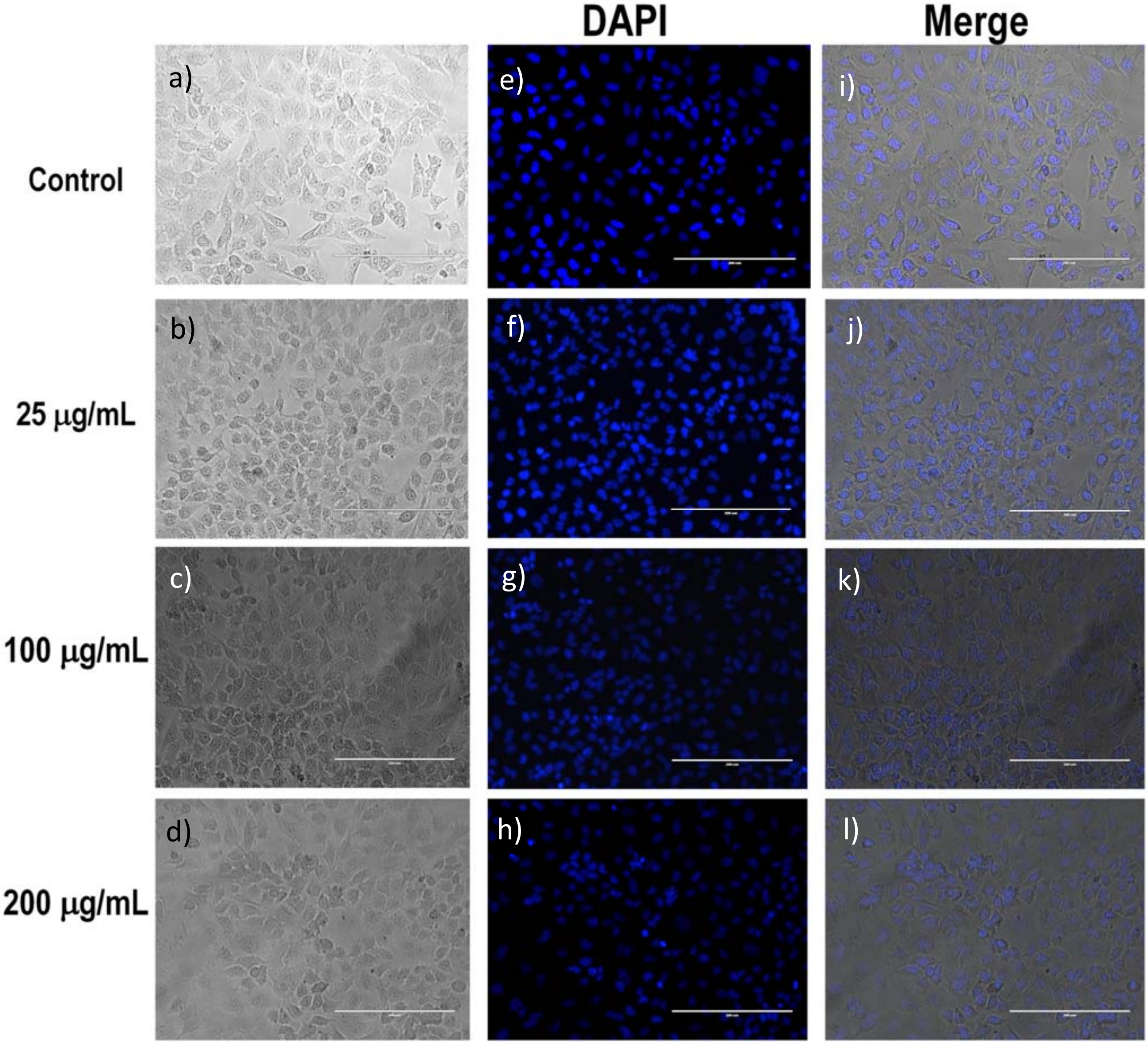

Figure S13. Comparison between fluorescence images of untreated (control) HeLa cells, and 24 h cultured cells with increasingly concentrated water dispersions of the C@1S@2S@i3S nanoprobe. Bright field: a) Control cells; b) and c) and d) Cells cultured with 25, 100 and 200 μg/mL water dispersions of the nanoprobe, respectively. Images for DAPI stained cells: e), f), g) and h), corresponding to a), b), c) and d), respectively. Combined images of those related in the left and middle columns appear in i), j), k) and l). Scale bars are for 200 μm.

Fluorescence microscopy images of MC3T3 cells stained with DAPI

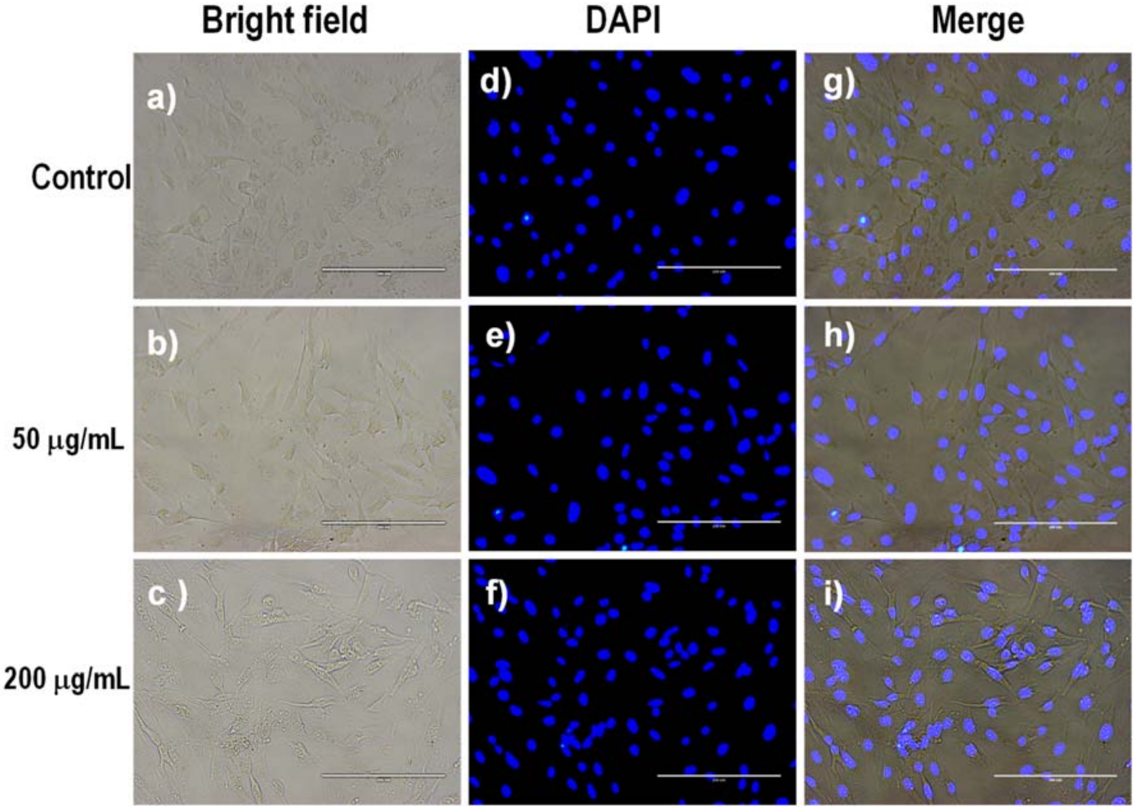

Figure S14. Comparison between fluorescence images of untreated (control) MC3T3 cells, and 24 h cultured cells with increasingly concentrated water dispersions of the C@1S@2S@i3S nanoprobe. Bright field: a) Control cells; b) and c) Cells cultured with 50 and 200 μg/mL water dispersions of the nanoprobe, respectively. Images for DAPI stained cells: d), e) and f), corresponding to a), b), and c), respectively. Combined images of those related in the left and middle columns appear in g), h) and i). Scale bars are for 200 μm.